ACS OMEGA

Open Access

http://pubs.acs.org/journal/acsodf

Article

Asphaltene Adsorption on Solid Surfaces Investigated Using Quartz Crystal Microbalance with Dissipation under Flow Conditions

Archana Jagadisan* and Sanjoy Banerjee

Cite This: *ACS Omega* 2024, 9, 15982−15995

Read Online

ACCESS | Metrics & More | Article Recommendations

ABSTRACT: Asphaltenes can cause operational challenges in petroleum production facilities and adversely affect production by adsorption on mineral surfaces and alteration of the oil wettability of reservoirs. Therefore, understanding asphaltene adsorption mechanisms and their effects is crucial to improving the efficiency of oil production and reducing costs. In this study, we focus on understanding the impact of asphaltene concentration and the depositing environment of asphaltene adsorption on solid surfaces using the quartz crystal microbalance with dissipation (QCM-D) technique. The initial and long-term kinetics of adsorption at different concentrations were examined on three different solid surfaces including silicon dioxide to represent quartz mineral, stainless steel, and gold. The frequency−dissipation data showed evidence of monolayer adsorption initially, followed by multilayer formation. At short times, the adsorbed mass increased linearly with time, suggesting that the process was kinetically controlled rather than diffusion-controlled. The results were reproducible and did not depend on convection velocity but did depend on the surface material. At later stages, the monolayer development appeared to follow the random sequential adsorption (RSA) theory. Once multilayer adsorption commenced, the rates agreed well with the two-layer model of Zhu and Gu, 1990. The impact of asphaltene adsorption on the wettability of the surface was examined using contact angle studies, which showed decreasing water wettability with an increase in the adsorbed mass. The contact angle of water after 12 h of adsorption leveled off at around 100° on all three surfaces. Contact angle measurements were also used to evaluate if brine salinity causes the wettability alteration of surfaces with the adsorbed asphaltene. The results indicate that at 3% NaCl solution, the contact angle decreased only slightly by less than 2°.

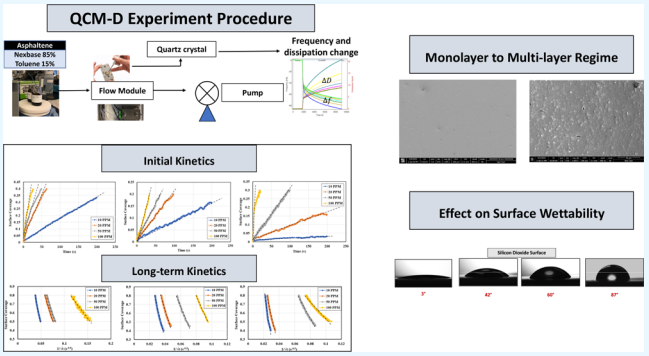

1. INTRODUCTION

Asphaltenes comprise heavy crude oil molecules containing compounds with a broad range of molecular weights, exhibiting increased polarization and surface activity.[1] Asphaltene molecules from various oils have been documented with weights ranging from several thousand to a few hundred grams per mole, typically falling between 40,000 and 300 g/mol.[2] However, it is widely acknowledged and accepted that petroleum asphaltenes typically exhibit a median molecular weight within the range of 550−750 g/mol.[3] They dominantly form sheet-like structures with one aromatic sheet system per molecule called the "island" model with interconnected heteroatoms.[4] A polarizable and surface-active fraction of crude oil, asphaltenes, is formed of polycyclic aromatic hydrocarbon sheet with peripheral chains,[3] which can adsorb on surfaces affecting oil−gas production and separation processes. Asphaltene adsorption mechanisms and the effects on interfacial properties are poorly understood and are under investigation. Asphaltenes are classified as a solubility class that dissolves in light aromatics but remains insoluble in paraffins.[5]

The adsorption of asphaltenes onto the mineral surfaces of reservoir rocks is recognized as one of the most destructive problems in the oil reservoir and challenges in oil reservoir management.[6−8] Wettability is the tendency of one fluid to spread on or adhere to a solid surface in the presence of other immiscible fluids.[9] One of the main factors found to influence the wettability alteration is the adsorption and deposition of polar and asphaltene fractions on the rock surface.[10−13] A shift in wettability toward a more oil-wet system was observed with an increase in polar and asphaltic fractions in crude oil.[13] The rupture of the water film on the rock surface and adsorption of asphaltenes were found to be the main cause of wettability alteration of the reservoir rock.[14] Furthermore, the adsorption of

Received: November 27, 2023
Revised: March 1, 2024
Accepted: March 6, 2024
Published: March 28, 2024

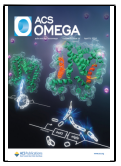

https://doi.org/10.1021/acsomega.3c09294
ACS Omega 2024, 9, 15982−15995

asphaltenes can lead to the fouling of pipelines, transportation equipment, as well as refining and upgrading facilities, resulting in reduced production efficiency and unexpected downtime.[15] Therefore, a better understanding of asphaltene adsorption and the effect of asphaltene adsorption on the wettability of solid surfaces is crucial for the better management of asphaltene impacts in oil production.

Adsorption of asphaltenes on solid surfaces has been studied using photothermal surface deformation spectroscopy,[16] UV spectrometry,[17−20] and a quartz crystal microbalance (QCM).[21−27] The mechanism and kinetics of asphaltene adsorption were found to strongly depend on the substrate and the type of interactions it can have with asphaltenes.[27] They show that polar interactions on hydroxyl-terminated surfaces result in a higher packing density, while alkane-functionalized surfaces exhibit a substantial delay in adsorption kinetics, and fluorinated surfaces show rapid monolayer formation.[27] The asphaltene structure was found to impact the adsorbed amount, and subfractions with increased aromaticity demonstrated higher tendencies for aggregation and adsorption/deposition.[28] Tavakkoli et al.[26] found that the initial adsorption process is controlled by adsorption kinetics and is at longer times governed by diffusion and convective transfer. Other studies found that the initial adsorption kinetics were diffusion-controlled.[24,29] At early times, asphaltene adsorption was found to be independent of flow rates, indicating a negligible effect of convective transfer on the adsorption process.[26,29] Despite this, there is no consensus on the kinetics of asphaltene adsorption on different metal surfaces. Moreover, the long-term adsorption kinetics have been relatively less researched and understood.

No straightforward relation was found between the adsorbed mass of asphaltenes and the surface coating based on the results from several reports,[21,24,26,29−31] which could be due to the use of different solvents and different asphaltene concentrations in these studies. The concentration of asphaltene solution,[19,24] the solvent used to dissolve asphaltenes,[24,32] and asphaltene polydispersity[26] are shown to impact the adsorbed mass of asphaltenes on solid surfaces. When the solvent and concentration were kept constant, Tavakkoli et al.[26] found that the mass adsorbed on carbon steel and iron oxide surfaces is higher in comparison to a gold surface. Cold lake and Athabasca asphaltenes are reported to have twice as high adsorption on stainless steel surface than on iron surface.[20] With an increase in heptane/toluene ratio, the corresponding amount of adsorbed mass increases due to a decrease in asphaltene solvent instability and formation of aggregates until a certain extent. A further increase in heptane ratio resulted in a decrease in adsorbed mass.[24,26] The formation of significant agglomeration and precipitation at a very low aromaticity of the solute is suggested as the cause of this phenomenon. The degree of surface wettability influences the deposited amount of asphaltene, where superhydrophobic coatings reduced asphaltene deposition.[33]

Several asphaltenes in toluene have been reported to exhibit multilayer adsorption on silica surfaces.[24,30,34,35] Liu et al.[24] found that the adsorption isotherm exhibited multiple regimes, suggesting a transition from monolayer to multilayer adsorption. Using QCM-D, Ekholm et al.[21] investigated the adsorption of asphaltenes and resins onto hydrophilic gold surfaces and reported that at moderate concentrations, asphaltenes form a hard layer on the surface. Ellipsometry measurements for asphaltene films on glass surface showed layer thicknesses ranging from 20 to 298 nm, which grew over time, suggesting multilayer formation.[35] The multilayer adsorption has been attributed to the formation of asphaltene aggregates.[17] When the water film on silica ruptures, toluene-solubilized asphaltene attaches to the silica surface, and the adsorption is irreversible.[36] The irreversibly adsorbed mass from asphaltenes in toluene was rigidly attached to silica, while weakly bound asphaltenes desorbed.[36] The fundamental physics of asphaltene adsorption mechanisms on solid surfaces is still poorly understood and warrants investigation.

One of the most commonly used enhanced oil recovery (EOR) techniques is water flooding,[37] which involves injecting water into the reservoir to push the remaining oil toward the production wells. However, the success of water flooding depends on the wettability of the rock surface.[38−42] One of the theories is that if the rock surface is oil-wet, water flooding can be ineffective because water tends to bypass the oil and flow through the rock pores without displacing the oil. In recent years, researchers have found that the salinity of water impacts the results of water flooding and that injecting low-salinity water into oil reservoirs can increase oil recovery. Some studies have shown that the low salinity water displaces the connate water and alters the surface properties of the rock, making it more water-wet.[41,43,44] This change in wettability reduces the capillary forces that trap oil in the rock pores, making it easier to displace and recover. However, the effect of salinity on the wettability of asphaltene surfaces is less explored and not understood clearly.

To better understand asphaltene adsorption on surfaces, we use QCM-D to perform an experimental study of asphaltene adsorption on stainless -steel, silicon dioxide, and gold. The aim is to investigate the impact of surface type and the effects of asphaltene concentration on adsorption kinetics. The silicon dioxide surface serves as a representative of the quartz rock surface, while stainless steel and gold are included in the study to assess the potential impact of the surface material on the adsorption process. We make an assumption that when the water film inside the rock pores ruptures, it creates conditions that are somewhat similar to adsorption onto dry rock surfaces. This is because, after the water film rupture, the rock surfaces are no longer in direct contact with the water phase, and they become available for interaction with other components, such as asphaltenes present in the crude oil. These asphaltenes can then adsorb onto the exposed rock surfaces. We also study the impact of asphaltene adsorption and brine salinity on the wettability of surfaces and how these relate to the amounts deposited. These investigations are meant to contribute to the management of asphaltene issues in upstream crude oil production by a better understanding of how asphaltenes are deposited on various surfaces and how the adsorbed asphaltenes affect wettability. Understanding the wettability changes induced by asphaltenes and the effect of brine salinity can help in developing effective EOR techniques that can increase the amount of oil recovered from reservoirs. Further work is being conducted on additives to the water flood to improve the water wettability of surfaces exposed to asphaltene adsorption and will be the subject of a subsequent paper.

Although the existing research in this field is extensive, a comprehensive understanding of the fundamental mechanisms behind asphaltene adsorption on solid surfaces remains limited. Current studies have often been confined to specific materials or kinetic stages. There is also a lack of consensus on the kinetics of asphaltene adsorption across various metal surfaces and timescales. This study introduces significant advancements in the understanding of asphaltene adsorption. This research

https://doi.org/10.1021/acsomega.3c09294
ACS Omega 2024, 9, 15982−15995

Table 1. Measured Density and Viscosity of Samples at a Temperature of 20 °C and Shear Rate of 100 s^{-1}

liquid	density (g/cm^3)	viscosity (mPa s)	ΔD (measured) (ppm)	ΔD (calculated) (ppm)	Δf (measured) (Hz)	Δf (calculated) (Hz)
85% Nexbase 2002 + 15% toluene	0.863825	0.545	117	113	−873	−848
toluene	0.771710	3.05	262	252	−1822	−1896

delves into the multidimensional kinetics of asphaltene adsorption, encompassing distinct temporal stages—early, intermediate, and extended time frames—offering a comprehensive exploration of this process. This study also explores multiple surfaces—stainless steel, silicon dioxide, and gold—to discern how various materials influence asphaltene adsorption kinetics, providing insights into material-specific behaviors. Additionally, it investigates the correlation between asphaltene adsorption and surface wettability alterations along with the impact of brine salinity on the asphaltene behavior. This research significantly bridges the gaps in understanding the relationship between the adsorbed asphaltene mass and the surface wettability.

2. EXPERIMENTAL SECTION

2.1. Materials. For the QCM-D studies, the asphaltenes are dispersed in a model oil phase that contained 15% toluene (99.8+%, ACROS Organics) and 85% aliphatic base oil by volume. The aliphatic base oil is chosen as the synthetic base oil of Nexbase 2002 from Neste Oil, Finland, which consists of oligomers of decane with different mass weights and is additive-free. The base oil is chosen because of its oxidation and temperature stability, in addition to nontoxicity. Without further purification, toluene (99.8+%, ACROS Organics) is used as the solvent. High-purity argon gas is used for drying after the cleaning process, and Millipore water is used for cleaning and rinsing. The viscosity of the model oil and toluene is measured using a 2° cone and plate configuration on a TA Instruments AR 2000 ex rotational rheometer at room temperature (298 K) at a shear rate of 100 s^{-1} and is given in Table 1. The shear rate is controlled by varying the rotational speed of the rheometer's spindle or the motion of the plates between which the material is sheared.

2.2. Sample Preparation. The asphaltene precipitation involved preparing a solution of crude oil and *n*-heptane in a ratio of 40:1 (v/m). This was sonicated for 60 min and left at room temperature for 24 h. Filtration occurred in two stages: 1200 mL filtered initially, followed by the addition of 10% of the initial volume of *n*-heptane for washing. After 45 min of sonication and 18 h of rest, a second filtration was performed. The filtered cake was washed with *n*-heptane for 5 days or until the solvent became colorless.[45,46] A stock solution containing 1000 ppm asphaltenes in toluene is made by sonicating it for 5 min, and then it is placed in a sealed glass vial for storage. To protect it from light exposure, the vial is covered by an aluminum foil. Before usage, the stock solution is sonicated for 5 min. Depending on the desired concentration in a 50 mL sample, the required amount of stock solution is diluted with toluene and then further diluted with Nexbase oil 2000 series. The prepared asphaltene solution is sonicated further for 5 min. The prepared solutions are discarded after 24 h to avoid bias caused by long-term phase segregation.

The choice of asphaltene concentrations used for this study was based on our insights into the aggregation behavior of asphaltenes in the model oil solution (85% aliphatic oil base and 15% toluene) in previous research findings.[47] Using liquid-state ^{1}H NMR, we found a distinctive change in the trend of the slope of mass fraction dependence of the NMR asphaltene signal. We observed a consistent linear increase in the asphaltene signal with respect to the asphaltene mass fraction, maintaining this trend until reaching 80 ppm. Beyond this concentration, while the signal continued to rise, the rate of increase notably slowed down, persisting up to the maximum mass fraction tested, which was 500 ppm. This observation notably contributes to our understanding and supports the determination of the critical nanoaggregation concentration (CNAC) of asphaltene in the model oil to be approximately 80 ppm. Therefore, in lower asphaltene mass fractions (below the apparent CNAC in model oil, i.e., below 80 ppm), it is anticipated that there will not be further aggregation. Conversely, at higher mass fractions (exceeding 80 ppm), there is a likelihood of more aggregate formation or, potentially, the initial aggregates may begin to flocculate. Moreover, our dynamic light scattering (DLS) data further corroborate these insights, revealing the particle size changes that align with our expectations.[47] Notably, immediately post-mixing, all solutions showed particle sizes of ∼75 nm and are found to be largely independent of the mass fraction. Over time, the particle size increases for asphaltenes above 80 ppm, while sizes remain almost stable below this concentration. In our current experiments, we have deliberately maintained concentrations below this critical threshold. This strategic choice was made to avoid aggregation effects and ensure the stability of asphaltene properties throughout our investigations. The decision to discard the prepared solutions after 24 h is primarily precautionary and based on the available DLS data, which extends up to 200 min.

2.3. Theory of QCM-D. Real-time kinetic study of the adsorbed mass and viscoelastic characteristics of adsorbed films is possible with the QCM-D system. The fundamental principle of QCM-D is that a piezoelectric sensor is excited to resonance by the application of an alternate voltage, and the resonance frequency, *f*, is measured and recorded as a function of time. Changes in frequency, Δf, give information on the deposited mass on the sensor surface, which can be used to examine the surface−molecule interaction such as molecular adsorption. In addition to monitoring frequency changes, QCM-D measures the system's energy loss, or dissipation, *D*. The dissipation value reflects the mechanical properties of the surface-adhering layer. Dissipation in conjunction with frequency can be used to quantify the mass, thickness, and viscoelastic properties of the soft layers. This capability enables QCM-D to assess adsorption kinetics and experiments and detect a change from a monolayer to an aggregate multilayer.

The contribution to the frequency (f) of the sensor crystal due to mass loading caused by the adsorption of rigid films can be calculated using the Sauerbrey equation.[48]

Mass loading:

$$\Delta f_{\text{adsorption}} = -\frac{n\Delta m}{C} \quad (1)$$

where *C* is a constant of the quartz crystal (17.7 ng/Hz cm^2 for a 5 MHz crystal), *n* is the number of the overtone, and Δm is the

https://doi.org/10.1021/acsomega.3c09294
ACS Omega 2024, 9, 15982−15995

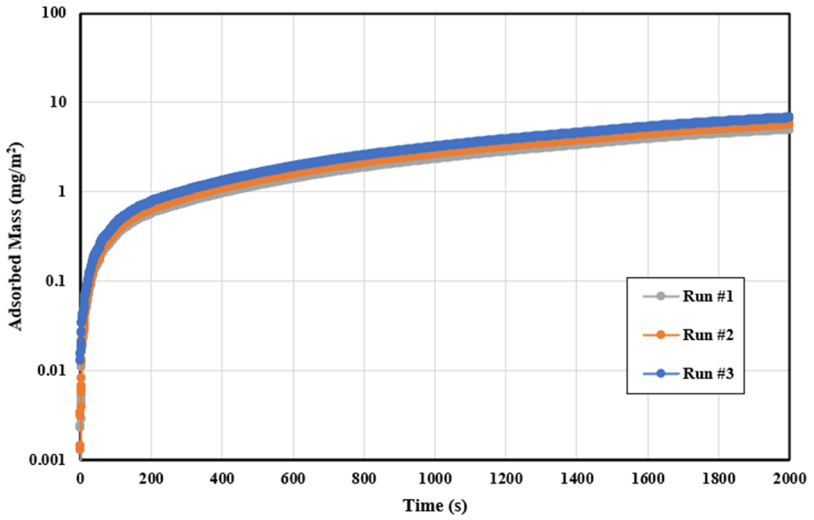

Figure 1. Repeatability of the adsorbed asphaltene mass on a quartz surface (3 runs) under flow conditions.

adsorbed mass. This relation holds true if the adsorbed molecules are equally distributed, and the adsorbed mass is minimal relative to the crystal itself.

In QCM, an overtone refers to a harmonic frequency of oscillation that is a multiple (whole number) of the fundamental resonance frequency of the crystal. The fundamental frequency is the first harmonic, and overtones are higher harmonics that have frequencies at integer multiples of the fundamental frequency. The increased frequency of higher overtones, such as the third overtone, makes them more sensitive to small mass changes on the crystal's surface. Consequently, they can detect even subtle interactions or changes, such as the adsorption of molecules, with greater precision. However, very high overtones also tend to have weaker signals. This means that while they can detect very small mass changes, they may produce signals that are more challenging to measure accurately, especially in the presence of noise. The choice of the third overtone is a common practical compromise that provides a good balance between the sensitivity and signal quality for many QCM experiments. For this reason, we use the third overtone for the calculations in this paper.

The shift in frequency is influenced by the adsorption of molecules as well as the liquid that carries the solid molecules through the flow module and the liquid trapped inside the adsorbed molecules. The contributions of liquid loading[49,50] and liquid trapping[50] to the frequency and dissipation of the crystals because of the adsorption of a rigid film can be calculated using the following equations

Liquid loading:

$$\Delta f_{\text{liquid-loading}} = -\sqrt{\frac{n}{\pi}}\frac{f_0^{3/2}}{\rho_q v_q}\left(\sqrt{\rho_l \eta_l} - \sqrt{\rho_s \eta_s}\right) \quad (2)$$

$$\Delta D_{\text{liquid-loading}} = -\sqrt{\frac{1}{n\pi}}\frac{2f_0^{1/2}}{\rho_q v_q}\left(\sqrt{\rho_l \eta_l} - \sqrt{\rho_s \eta_s}\right) \quad (3)$$

Liquid trapping:

$$\Delta f_{\text{liquid-trapping}} = -\frac{2f_0^2}{\rho_q v_q} h_l(\rho_l - \rho_s) \quad (4)$$

where f_0 is the fundamental resonant frequency ($f_0 = 5 \times 10^6$Hz), ρ_q is the specific density of quartz (2650 kg/m^3), ν_q is the shear wave velocity in quartz (3340 m/s), μ_q is the shear modulus of quartz (2.947 × 1010 Pa), h_q is the thickness of the quartz crystal (3.37×10^{-4} m), h_l is the thickness of the trapped liquid, ρ is the density, η is the viscosity, and subscripts 's' and 'l' refer to the solvent and liquid mixtures, respectively.

2.4. QCM-D Experiment Procedure. The QCM-D instrument used for the experiments was from Biolin Scientific. Nanoscience-supplied silicon dioxide-coated quartz sensors (QXS 303), stainless steel sensors (QSX 304), and gold sensors (QSX 301) were used as the adsorbents. The sensors were cleaned before the experiment to ensure the accuracy and repeatability of the results. The cleaning procedure for the gold sensor involved performing UV/ozone treatment first for 10 min. This step is used to decompose any trace organic matter deposited on the sensor into volatile substances by UV rays, followed by strong oxidation, to remove contamination from the surface. This was followed by placing the sensor in a 5:1:1 heated mixture of Milli-Q water, ammonia (25%), and hydrogen peroxide (30%) to 75 °C. This was followed by rinsing with Milli-Q water, drying with nitrogen gas, and finally repeating UV/ozone treatment for 10 min. Similar recommended protocols from the manufacturer for cleaning the stainless steel and silicon dioxide sensors were followed prior to performing the adsorption experiments. Additionally, each sensor was used no more than five times to ensure repeatability. The sensors are transferred to a flow module (QFM 401) after cleaning, which is connected to a peristaltic pump.

For asphaltene adsorption experiments, first, the reference solvent (85% Nexbase 2002 + 15% toluene) was injected through the flow module at 50 μL/min for about 2 h, until a stable baseline is achieved. Once a stable baseline is achieved, the inlet is then switched to the freshly prepared asphaltene solution placed on a sonicator, and a new measurement is started. The changes in resonant frequency and dissipation kinetics of the first, third, and fifth overtones were measured and recorded simultaneously. The waste is collected at the other end of the flow module and disposed off. The tubing from the peristaltic pump to the flow module is cleaned between experiments. After each test, the flow module is cleaned by flushing with toluene, drying in air, and then cleaning with 1 wt % sodium dodecyl sulfate solution in deionized water. The module is then rinsed

https://doi.org/10.1021/acsomega.3c09294
ACS Omega 2024, 9, 15982−15995

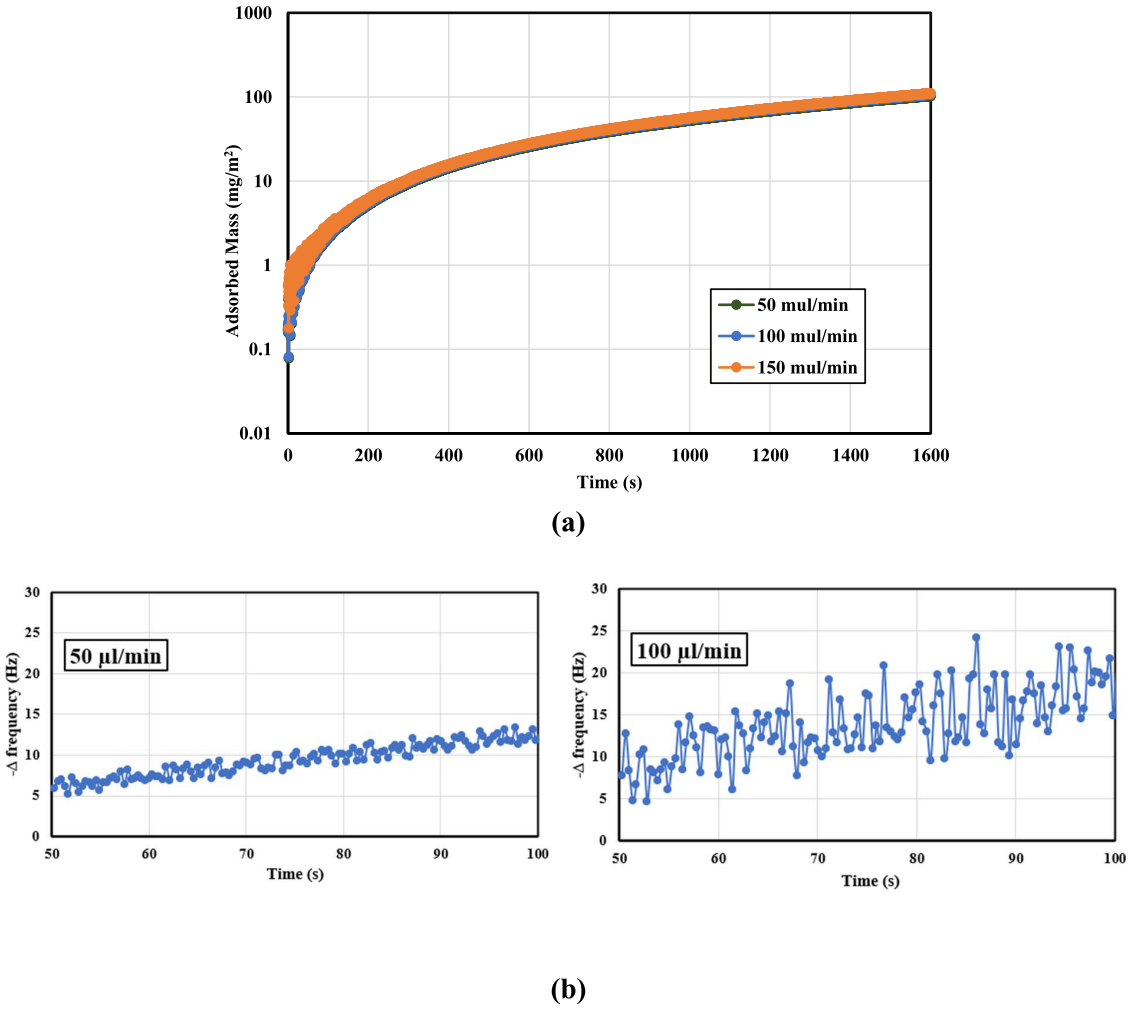

Figure 2. (a) Effect of the flow rate on the amount of adsorbed asphaltene mass onto a gold crystal surface vs time at different flow rates. (b) Close-up of change in frequency vs time for 50 and 100 μL/min.

with deionized water and dried with argon gas. Asphaltene solutions of increasing concentration from 10 to 50 ppm were injected sequentially on the sensor.

2.5. Measurement of Contact Angle. An Attension Theta Optical Tensiometer is used for contact angle measurements on the sensor surface. Contact angle measurements are used to characterize the wettability of the sensor surface. The sessile drop method is used to determine the wettability of the surface. In a sessile drop measurement, a droplet of a few microliters in volume is deposited onto the sensor surface (stainless steel and quartz sensors) and imaged by an optical camera. Edge detection is used to identify the droplet shape from the image of the droplet and is then analyzed by software to determine the contact angle between the droplet and the baseline surface material. The contact angle is averaged over a period of 5 min, and the contact angle on the right and left sides of the droplet is averaged.

3. RESULTS AND DISCUSSION

3.1. Validation of the QCM-D Experiment. The frequency and dissipation change of liquids introduced in the QCM-D chamber are calculated from the Sauerbrey equation in Section 3.3. The experimentally determined values of frequency and dissipation for pure solvent mixtures composed of toluene and a mixture of 85% Nexbase 2002 and 15% toluene using the previously described experimental procedure are compared against theoretically calculated values. Table 1 shows a comparison of experimental and theoretical values of frequency change and dissipation data. It can be seen that the experimentally determined values agree well with the corresponding theoretically computed values. The relative error between the measured and calculated values are within ±3.9%. This provides validation for the applicability of the QCM-D setup and experimental procedure. The third overtone is considered for Δf and ΔD.

Figure 1 shows three QCM-D experimental runs on the quartz surface for 20 ppm asphaltene solution under flow conditions. Runs #1 and #2 closely overlap, while Run #1 shows an average error of less than 1 mg/m^2 adsorbed mass. This shows that the experiments are repeatable and provide quality control on the experimental results.

3.2. Impact of Flow Rate on Adsorption. To examine the impact of convective transfer on the asphaltene adsorption process, QCM-D experiments are conducted at varied flow rates. Figure 2a shows the results for 50 ppm asphaltene solution at three flow rates, 50, 100, and 150 μL/min. The adsorbed mass of asphaltenes is displayed in the plot. Figure 2 shows that the rate of adsorption is nearly independent of flow rates, indicating that convective transfer has little impact on the adsorption process.

https://doi.org/10.1021/acsomega.3c09294
ACS Omega 2024, 9, 15982−15995

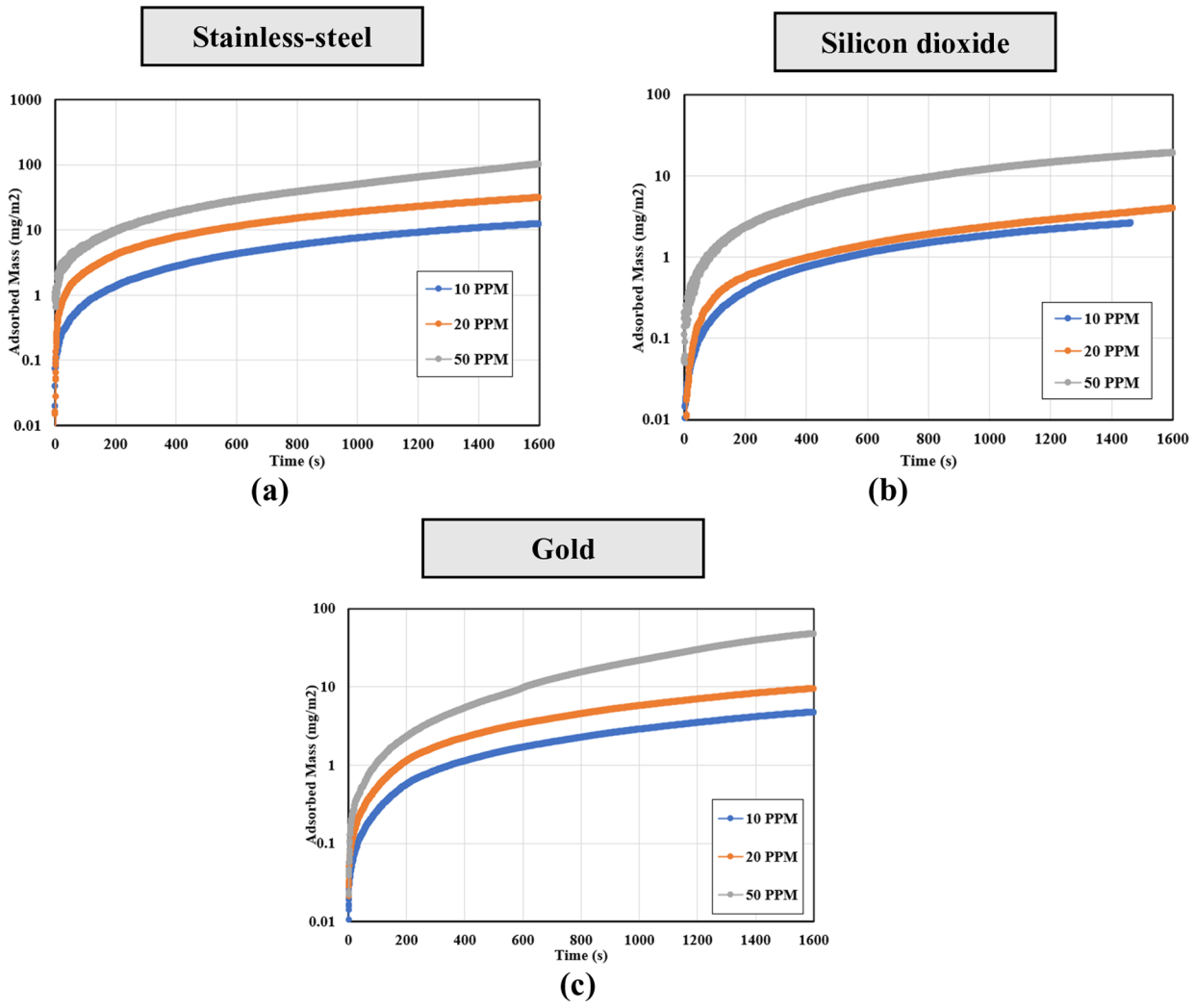

Figure 3. Adsorption kinetics of different concentrations (10−50 ppm) of asphaltene dissolved in toluene (15 v/v %) and Nexbase (85 v/v %) on (a) stainless steel, (b) quartz, and (c) gold surfaces.

Figure 2b shows the fluctuation of the resonance frequency of the QCM sensor in contact with the flowing asphaltene solution pumped using the peristaltic pump for two different flow rates, 50 and 100 μL/min. The results show that smaller frequency fluctuation is observed for lower flow rates, whereas higher flow rates result in higher fluctuations. The smaller fluctuations at lower flow rates could be attributed to the cyclic pressure change as the peristaltic pump head rotated. For higher flow rates, a release of accumulated pressure could cause a big frequency change of the resonance frequency. Although, on average, the results did not vary significantly between different flow rates, the noise increases with higher flow rates. Therefore, we use the lowest flow rate in the peristaltic pump, 50 μL/min, as the flow rate for our experiments.

3.3. Adsorption on Solid Surfaces. The adsorption kinetic curves of asphaltene in model solutions on three different surfaces (stainless steel, silicon dioxide, and gold) are shown in Figure 3. The adsorbed mass of asphaltenes can be seen to increase with the increase in time, irrespective of the asphaltene concentration in the solution. The adsorption initially undergoes a rapid increase and then slows down at later times. For both low- and high-concentration asphaltene solutions, the adsorbed amount increases with the increasing time for the time frame of the experiment.

Figure 4 shows a comparison of asphaltene adsorption on stainless steel, silicon dioxide, and gold surfaces. The results show that for the same concentration, a higher amount of asphaltene is adsorbed on stainless steel and gold surfaces as compared to the silicon dioxide surface at lower concentrations. At 50 ppm asphaltene concentration, the adsorbed mass on gold and stainless steel surfaces is similar after longer times, while the quartz surface has a lower amount adsorbed. The adsorbed amounts observed in our experiments are orders of magnitude higher than those observed by Hu et al.[36] and Gonzales and Taylor.[51] This discrepancy arises from the different experimental conditions. In their studies, asphaltene was dissolved in toluene for the measurements. In contrast, our experiments involve dissolving asphaltenes in a model oil and toluene solution to simulate reservoir conditions. It is worth noting that the adsorbed mass of asphaltenes is significantly influenced by the solute. In some of our additional experiments (not reported in this paper), where toluene was used as the solute, the adsorbed mass was an order of magnitude lower.

Figure 5 shows asphaltene adsorption on the surfaces after very long times for 50 ppm solution (12 h). We see that the adsorbed mass equilibrates at different adsorbed amounts, with the adsorbed mass on gold and stainless steel being nearly equal and that on quartz being lower. The rate of change of adsorption

https://doi.org/10.1021/acsomega.3c09294
ACS Omega 2024, 9, 15982−15995

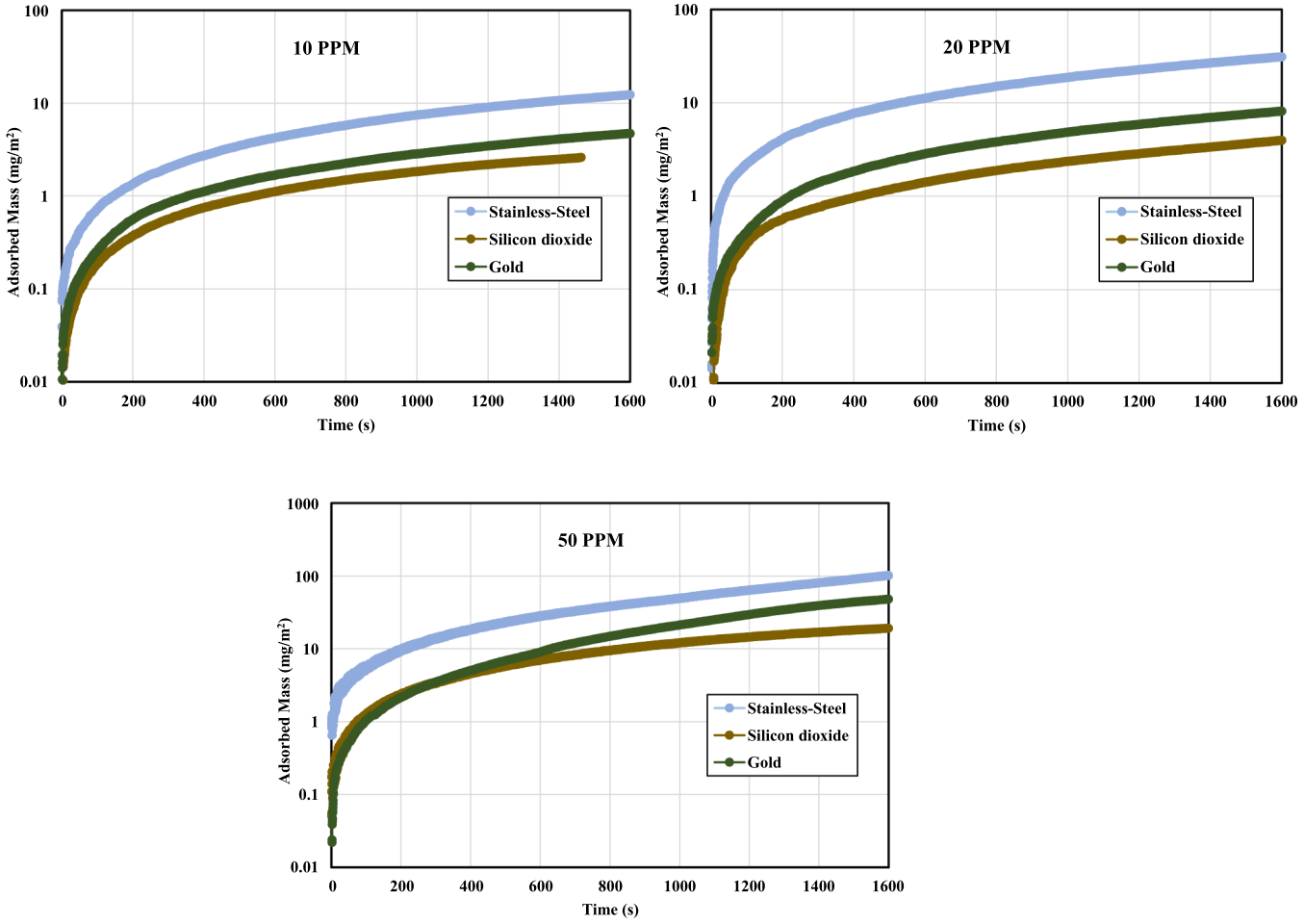

Figure 4. Comparison of asphaltene adsorption on stainless steel, silicon dioxide, and gold surfaces.

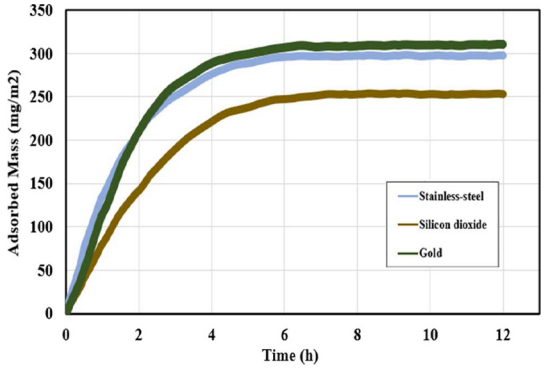

Figure 5. Comparison of long-term asphaltene adsorption on stainless steel, silicon dioxide, and gold surfaces for 50 ppm concentration.

is very low in the last 4 h of the experiment and is nearly the same for all the surfaces, indicating that the adsorption kinetics become independent of the surface effect.

3.4. Single-Layer vs Multilayer Analysis of Asphaltene Adsorption. In QCM, materials in contact with the oscillating sensor surface will cause energy losses. Liquids and soft films in contact with the surface will deform during the oscillation, causing the system to lose energy. Energy losses caused by thin and rigid layers are lower than those caused by soft and/or thick layers because they do not flex during oscillation. As a result, high dissipation means that the material in touch with the surface is soft or viscous, whereas low dissipation means that the material at the surface is rigid and oscillates. For $|\Delta D/(\Delta f/n)| \ll 4 \times 10^{-7}$ Hz^{-1}, the surface can be treated as sufficiently thin, and the Sauerbrey equation is valid.[52,53] This value comes from considering the ratio of dissipation change and frequency change obtained as a solution to the viscoelastic wave equation with no slip boundary conditions.[54]

Figure 6a–c shows the plot of dissipation change plotted against frequency change at different concentrations on three solid surfaces. The ratio of dissipation change to frequency change is compared to the reference line $|\Delta D/\Delta f| = 4 \times 10^{-7}$ Hz^{-1}. It can be seen that the curves fall below the reference line initially, regardless of the concentration or surface type. Moreover, at initial times and low frequency changes, the dissipation–frequency curves fall in the same line for different concentrations, indicating that the molecules adsorbed on the sensor surface form films with similar structures or properties. At higher frequency changes, the dissipation-to-frequency ratio increases beyond the reference line. This shows that asphaltene layers are becoming softer with more asphaltenes deposited on the surface of the sensor, potentially indicating a shift from monolayer to softer multilayer formation of asphaltenes around 25–40 Hz, which is around 4.5–7 mg/m^2. The adsorbed mass of 3.2–6 mg/m^2 has been widely reported in the literature to correspond to a monolayer adsorption regime.[7,24,29,31,55−57] For the subsequent sections on the kinetics of adsorption, we focus on the monolayer adsorption regime.

Liu et al.[24] found that asphaltene adsorption could be modeled by a two-step model. The two-step adsorption model,

https://doi.org/10.1021/acsomega.3c09294
ACS Omega 2024, 9, 15982−15995

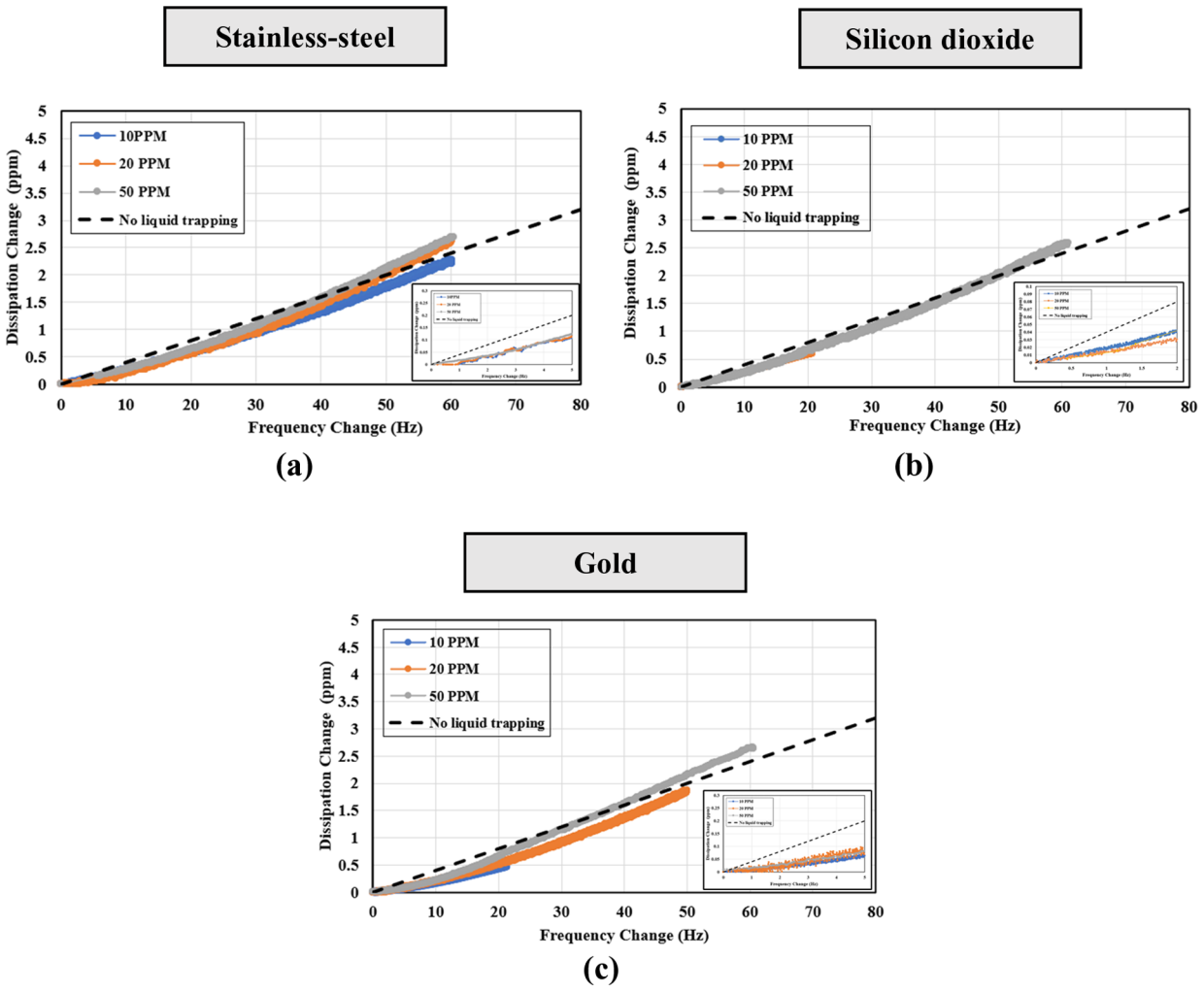

Figure 6. Dissipation vs frequency change plot for adsorbed asphaltenes at different concentrations on (a) stainless steel, (b) silicon dioxide, and (c) gold surfaces.

originally proposed by Zhu and Gu in 1990[58] (referred to as the ZG model), provides an explanation for the deposition of asphaltene molecules onto solid surfaces. According to the model, the deposition occurs in two steps. In the first step, asphaltene monomers are adsorbed onto hydrophilic surfaces via interactions between the π-electrons of polyaromatic hydrocarbon rings and the surface. This step can lead to the formation of a Langmuir monolayer on the solid surface, similar to asphaltene adsorption onto the liquid/liquid interface observed in previous studies.[3,59−62] In the second step, the adsorption increases significantly as the freshly adsorbed molecules interact with previously adsorbed molecules to form aggregates on several active sites. The binding energy between the already adsorbed and the next layer of adsorbing molecules decreases significantly due to weak interactions between the alkyl chains of the polyaromatic hydrocarbons and the physisorption of the aggregates, which tend to be voluminous and loose. This creates a large space between adsorbed molecules, which can accommodate and trap more fluid and increase dissipation during oscillations.

Asphaltene molecules are suitable for this two-step adsorption model because of their amphiphilic characteristics, which allow them to adsorb onto a liquid/liquid interface or aggregate in the solution. The ZG model has been shown to be successful in fitting experimental data in earlier studies on asphaltene adsorption from toluene onto reservoir rock surfaces such as dolomite and Berea sandstone.[63] The adsorption isotherm is calculated according to eq 5,[58]

$$\Gamma = \frac{\Gamma^{\infty} k_1 C\left(\frac{1}{n} + k_2 C^{n-1}\right)}{1 + k_1 C(1 + k_2 C^{n-1})} \tag{5}$$

where Γ is the amount of adsorbed molecules, Γ^{∞} is the maximum possible adsorption at high concentrations, k_1 is the first adsorption step parameter (i.e., the adsorption of asphaltenes in solution to the solid surface), k_2 is the second adsorption step parameter (i.e., the adsorption of asphaltenes in solution to those asphaltene molecules that have already adsorbed to the solid), C is the bulk concentration, and n is the mean aggregation number of the adsorbed molecules. When k_2 becomes negligible, the equation becomes a Langmuir-type adsorption isotherm. By using the ZG model and fitting it with experimental data, the maximum surface coverage and adsorption parameters can be numerically computed through the optimization process.

Figure 7 shows the adsorbed mass obtained from asphaltene solutions at various concentrations along with the fitting curves obtained using the optimized adsorption parameters and the maximum mass surface coverage obtained from the two-step deposition model (i.e., the ZG model). The figure indicates that

https://doi.org/10.1021/acsomega.3c09294
ACS Omega 2024, 9, 15982−15995

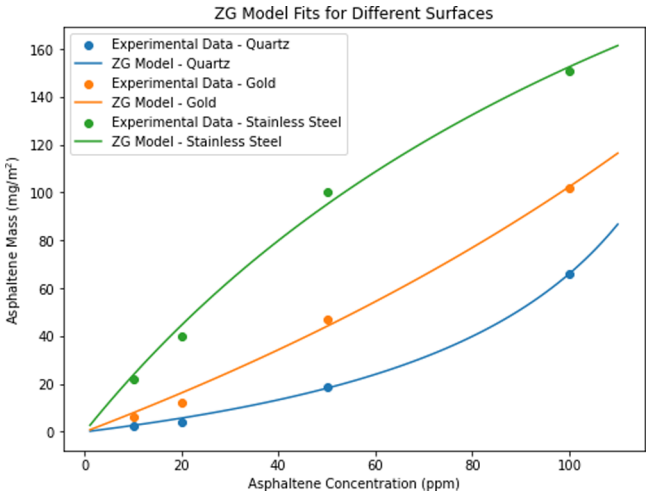

Figure 7. Adsorption isotherm of asphaltene on gold, stainless steel, and silicon-dioxide vs ZG model fit.

the ZG model can effectively model the adsorbed mass characteristics on different surfaces.

3.5. Asphaltene Structure and Morphology. To get an idea of how the adsorbed films look, the sensor surfaces were scanned using scanning electron microscopy (SEM) after 30 min of adsorption at different concentrations. Figure 8 illustrates the SEM images captured at a magnification of 1000 times, illustrating the adsorption of asphaltene on a gold-coated QCM surface at two different concentrations, 10 and 50 ppm. The SEM images show that the surface at lower concentrations appears to be more uniform and smoother, while the image at higher concentrations has more heterogeneity and variations in thickness, with a rougher texture. This observation suggests that the adsorption of asphaltene at higher concentrations may occur in multiple layers, leading to varying thicknesses and a rougher surface texture. In contrast, the adsorption at lower concentrations appears to be a monolayer, leading to a more homogeneous and smoother surface.

3.6. Initial Adsorption Kinetics. The adsorption kinetics data are further examined in order to gain a better understanding of how asphaltenes begin to deposit onto solid surfaces. Figure 9a–c shows a plot of the surface coverage for four different concentrations of asphaltenes versus time on stainless steel, silicon dioxide, and gold surfaces, respectively. The plot shows that the surface coverage (which is proportional to adsorbed mass) for all concentrations of asphaltenes on all three surfaces varies linearly with time. After initial times, some curves can be seen deviating from linearity, indicating that different kinetics affect adsorption.

From the Filippov quantitative theory of kinetic–diffusive–convective adsorption in a flow cell,[64] the surface coverage (Γ) of adsorbed molecules for adsorption kinetics can be calculated as follows

$$\frac{\partial \Gamma(x,t)}{\partial t} = R^+ - R^-,\ R^+ = K_{ad}R_1(c(0,t),\Gamma),\ R^- = K_{des}R_2(\Gamma) \tag{6}$$

$$\frac{\partial \Gamma(x,t)}{\partial t} = K_{ad}[c(x,0,t)]^m[\Gamma_m^0 - \Gamma(x,t)]^r - K_{des}\Gamma(x,t) \tag{7}$$

where R^+ and R^- are the forward and backward rates in kinetic expression, Γ_m^0 is the maximum adsorption, $c(x, 0, t)$ is the surface concentration, $\Gamma(x, t)$ is the adsorbed amount per unit surface, m and r are the parameters of adsorption and desorption kinetics, and K_{ad} and K_{des} are the rate constants for adsorption and desorption, respectively.

Therefore, as per the Filippov model,[64] if the slope of adsorption versus time is a linear function of time for initial times, then the adsorption process is controlled by the adsorption kinetics (eq 3).

$$\Gamma(t) = St \tag{8}$$

where

$$S = K_{ad}c_0^m(\Gamma_m^0)^r \tag{9}$$

S is the slope, c_0 is the adsorbate concentration in the bulk, and K_{ad} is the rate constant of adsorption.

From Figure 9, we can see that at initial times, the surface coverage is a linear function of time, indicating that the rate of adsorption depends on K_{ad} and does not depend on the diffusion-controlled regime. Therefore, the adsorption process is controlled by adsorption kinetics. Additionally, it can be seen that at low concentrations, the linearity of surface coverage and

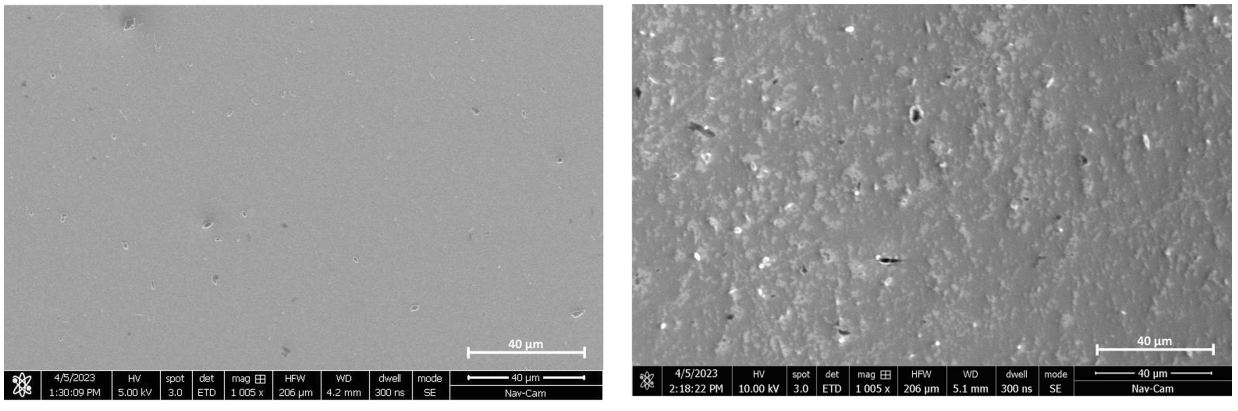

(a) **(b)**

Figure 8. SEM images of asphaltene adsorption on a gold-coated QCM surface at 1000 times magnification at asphaltene concentrations of (a) 10 and (b) 50 ppm.

https://doi.org/10.1021/acsomega.3c09294
ACS Omega 2024, 9, 15982–15995

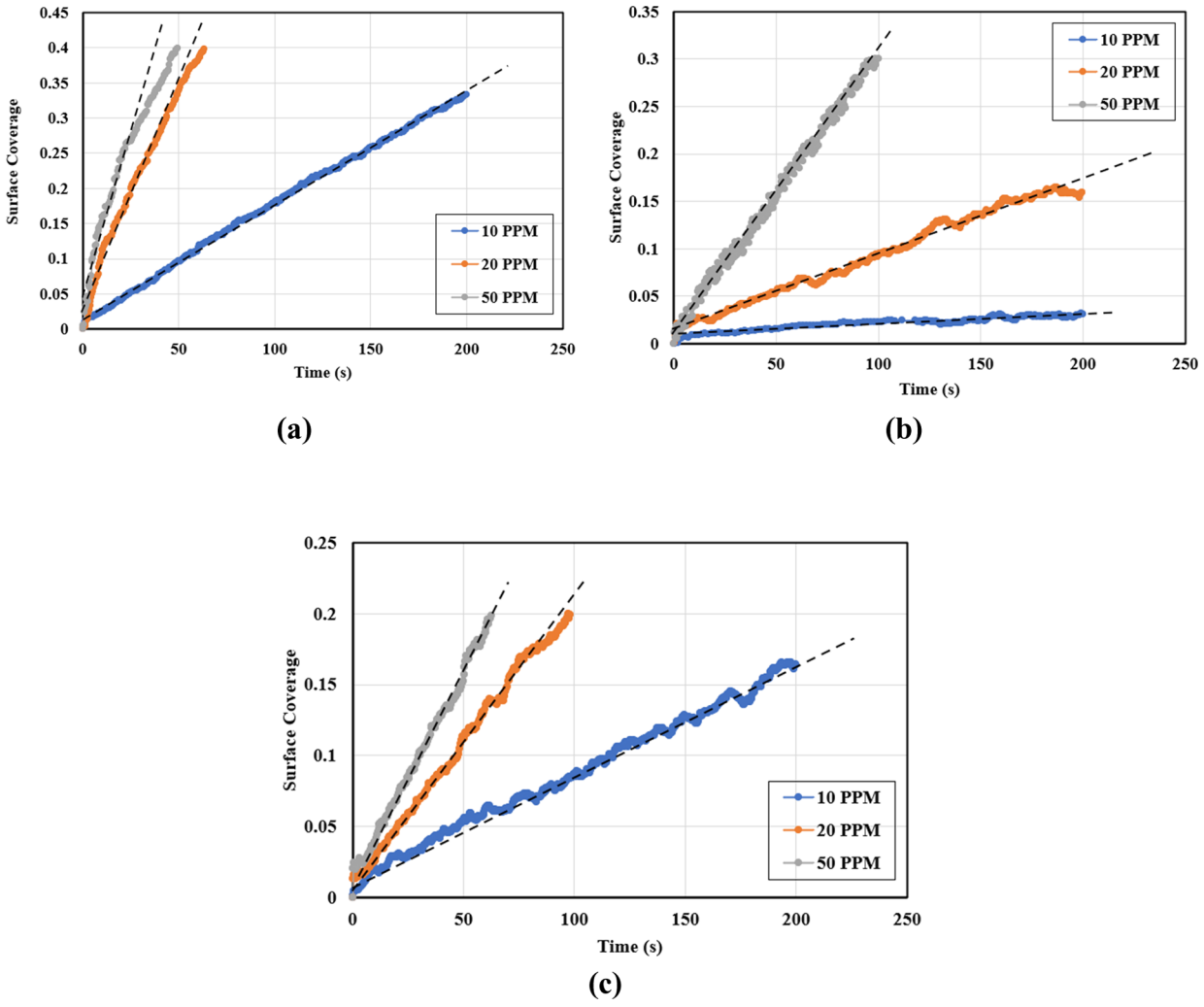

Figure 9. Dynamic adsorption vs time for asphaltenes at different concentrations on (a) stainless steel, (b) silicon dioxide, and (c) gold surfaces.

time remains for a longer time as compared to higher concentrations showing transition to different adsorption kinetics at earlier times for higher concentrations.

3.7. Long-Term Adsorption Kinetics. The adsorption kinetics data at longer times are examined in Figure 10a–c, which shows the plots of surface coverage of asphaltenes versus time on stainless steel, silicon dioxide, and gold surfaces, respectively. The plot shows that the surface coverage for all concentrations of asphaltenes on all three surfaces follows a power law behavior of $\sim 1/\sqrt{t}$.

A previous study on the kinetics of asphaltene adsorption at longer times and higher interfacial coverage indicates that when coverage reaches 35–40%, the surface coverage evolution for isotropic or quasi-isotropic particles in a random sequential adsorption (RSA) regime follows a linear dependency of surface coverage on $1/\sqrt{t}$. The asymptotic time variation of the surface coverage has been derived[65−67] as follows

$$\frac{\Gamma(t)}{\Gamma_\infty} = \frac{\Gamma_{jam}}{\Gamma_\infty} - \frac{K}{\sqrt{tk_aC}} \quad (10)$$

where Γ_{jam} is the jamming limit, K is the geometrical constant, k_a is the adsorption rate constant, and C is the concentration. However, for anisotropic noncircular particles as well as for nonaligned squares and rectangles, the surface coverage has been found to vary as a power of $\sim t^{(-1/3)}$. To estimate the jamming limit in our data, a reliable estimate of the size and shape of the asphaltene molecules used in this study is required.

For irreversible RSA with diffusional relaxation, the surface coverage was found to depend on the deposition probability (p) or diffusion probability $(1-p)$.[68] It was found that the empty-area fraction decays according to $1-\theta(t) = B(1-p)^a p^b (pt)^{-0.5}$ for RSA with diffusional relaxation, where θ is the surface coverage fraction, a and b are the fitting parameters, B is the proportionality constant, and t is the time.

3.8. Effect of Asphaltene Adsorption on Surface Wettability. To determine the impact of asphaltene adsorption on the wettability of the solid surface, contact angles were measured on the surfaces after they were dried down. The results are shown in Figure 11. The results suggest that the contact angle increases with increasing asphaltene concentration and adsorbed mass for all of the surface types.

Among the different surface types, we see that the silicon dioxide surface shows a less pronounced increase in contact angle as compared to gold or stainless steel surfaces. This could be because the adsorbed mass is relatively lower on silicon dioxide surfaces as compared to the other two surfaces (Figure 4). This indicates a direct correlation between the adsorbed mass content on the surface and the wettability of the surface; i.e., an increase in asphaltene mass adsorbed is directly

https://doi.org/10.1021/acsomega.3c09294
ACS Omega 2024, 9, 15982−15995

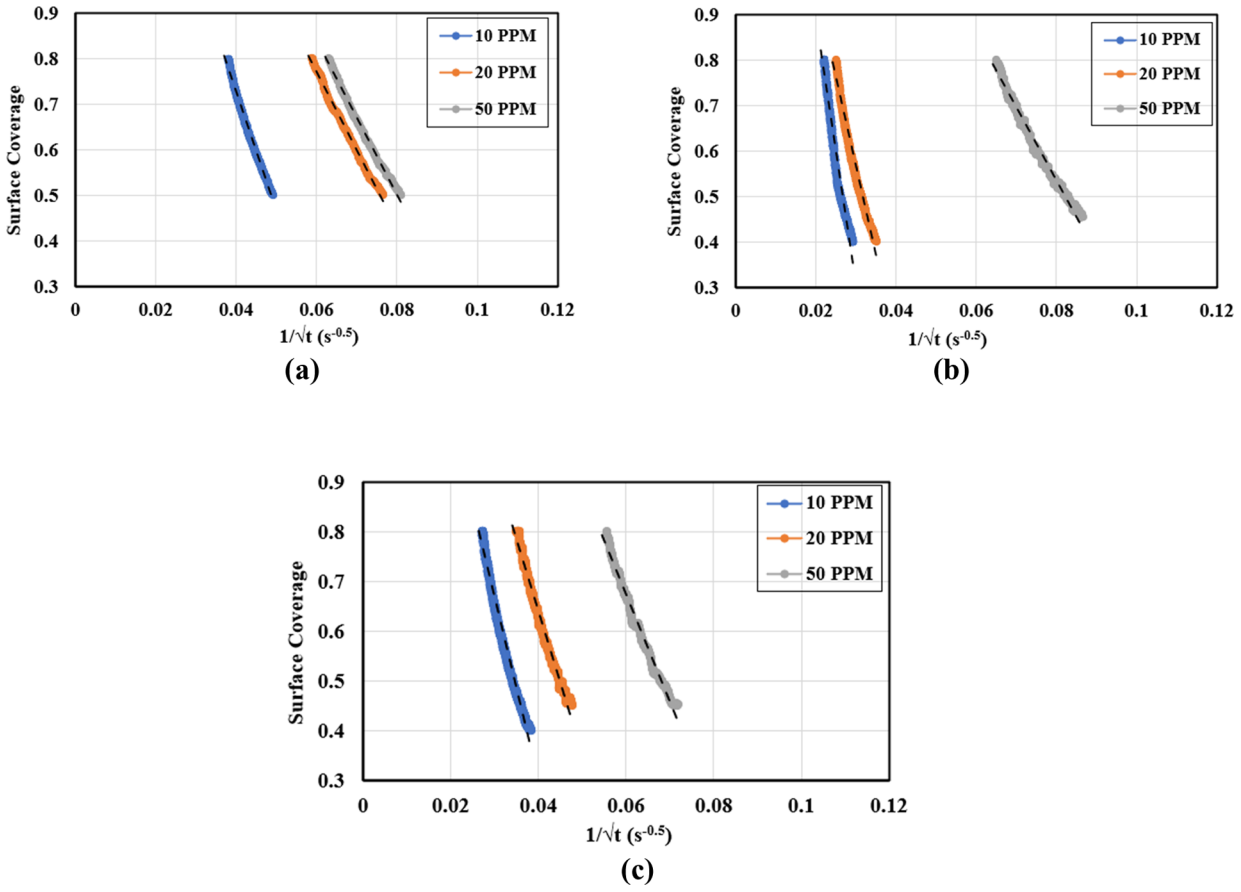

Figure 10. Surface coverage vs reciprocal of square root of time for different concentrations at longer times for dynamic adsorption vs time for asphaltenes at different concentrations on (a) stainless steel, (b) silicon dioxide, and (c) gold surfaces.

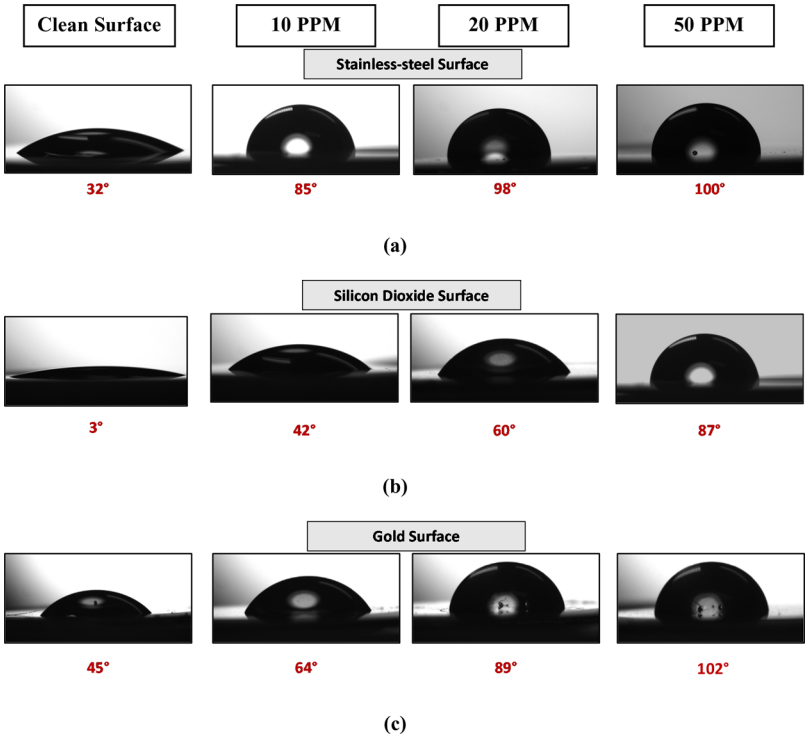

Figure 11. Contact angle of water droplet on (a) stainless steel, (b) silicon dioxide, and (c) gold surfaces after the adsorption of asphaltenes at different concentrations.

https://doi.org/10.1021/acsomega.3c09294
ACS Omega 2024, 9, 15982−15995

proportional to an increase in hydrophobicity of the solid surface. The heterogeneity in the wetting states of the surfaces suggests that complete coverage with asphaltenes without exposure to the surface has not yet been achieved.

Finally, we measure the contact angle of the surfaces after 12 h in the asphaltene solution. The results are shown in Figure 12.

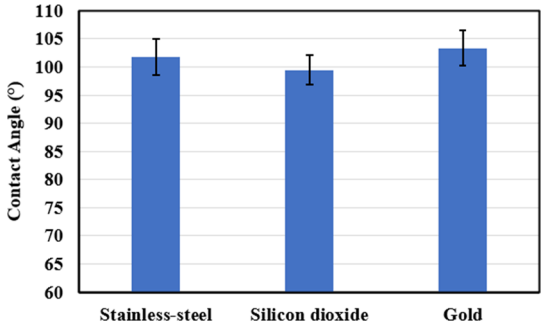

Figure 12. Contact angle of water droplet after 12 h in asphaltene solution on stainless steel, silicon dioxide, and gold surfaces.

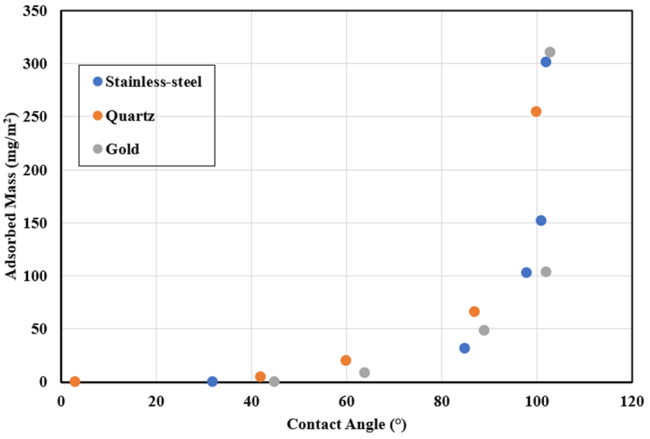

Figure 13. Contact angle of water droplet as a function of adsorbed mass for stainless steel, silicon dioxide, and gold surfaces.

Figure 13 shows the average values of contact angles measured as a function of the adsorbed mass. The results show that the contact angle on all three surfaces converges toward the same value ~100°. The wetting homogeneity of the three surfaces as well as little variation in the contact angles, as observed from the error bars, suggests that the surface effect is negligible on the complete and homogeneous coverage with asphaltenes.

The effect of salinity on wettability is tested with a high-salinity 3% NaCl solution, shown in Figure 14. The results show that the contact angle decreases slightly by 0.6°, 1.4°, and 0.3° on stainless steel, silicon dioxide, and gold surfaces, respectively. However, this change falls in the error range, and thus, the results are inconclusive. Therefore, there is a need for further investigation of the effect of different salinities on the wettability of asphaltene surfaces. A study on the change of interfacial tension (IFT) between crude oil and aqueous solutions using brine solutions with different salinities showed that the highest IFT is measured for DI water/oil system and shows a slight decrease in IFT for high-salinity brine/oil system.[69,70] The lowest IFT is measured for low-salinity brine/oil systems. A corresponding change was seen in the contact angles, where

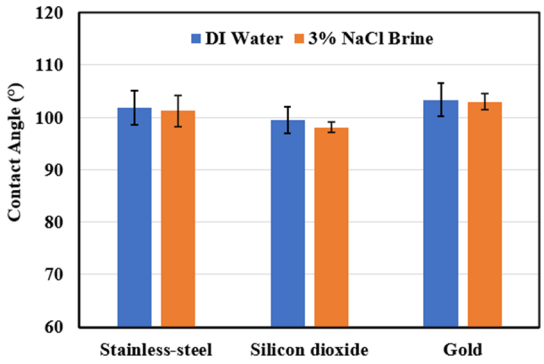

Figure 14. Contact angle of water droplet after 12 h in asphaltene solution on stainless steel, silicon dioxide, and gold surfaces.

there was a wettability alteration from oil-wet to water-wet in low-salinity brines.

4. CONCLUSIONS

QCM-D technique was used to study the kinetics of adsorption of asphaltenes in a model oil solution onto stainless steel, silicon dioxide, and gold surfaces at a concentration range of 10−50 ppm. The findings demonstrate that for the same concentration, more asphaltene was adsorbed on gold and stainless steel surfaces than on silicon dioxide surfaces. A change in the slope of dissipation versus frequency data was observed ~4.5−7 mg/m^2 of adsorbed mass, indicating a transition from the monolayer to multilayer regime. In the monolayer regime, initial adsorption kinetics were found to be consistent with the kinetics controlled on all three surfaces. At longer times during the monolayer formation period, the surface coverage for all the concentrations of asphaltenes on all three surfaces followed a power law behavior $\sim 1/\sqrt{t}$ consistent with the random sequential adsorption (RSA) regime. When multilayer formation commenced, adsorption agreed with the two-layer model of Zhu and Gu.[58] The wettability of asphaltene was found to have a direct correlation with the amount of asphaltene adsorbed on the sensor surface during the monolayer formation period when there was incomplete surface coverage. A higher asphaltene adsorption was found to make the sensor surface more hydrophobic. At longer adsorption of around 12 h, the surface type had negligible effect, and the contact angle of water droplets on the surfaces converged to ~100°. High-salinity brine did not show a significant effect on the wettability of asphaltene surfaces.

AUTHOR INFORMATION

Corresponding Author

Archana Jagadisan − *Energy Institute and Department of Chemical Engineering, City College of New York, New York, New York 10031, United States;* orcid.org/0000-0002-3128-8559; Email: akaniyanoorjagadis@ccny.cuny.edu

Author

Sanjoy Banerjee − *Energy Institute and Department of Chemical Engineering, City College of New York, New York, New York 10031, United States*

Complete contact information is available at: https://pubs.acs.org/10.1021/acsomega.3c09294

Notes

The authors declare no competing financial interest.

https://doi.org/10.1021/acsomega.3c09294
ACS Omega 2024, 9, 15982−15995

■ ACKNOWLEDGMENTS

This research was supported by the National Science Foundation under Grant No. 1743794, PIRE: Investigation of Multi-Scale, Multi-Phase Phenomena in Complex Fluids for the Energy Industries.

■ REFERENCES

(1) Hassanzadeh, M.; Abdouss, M. Essential role of structure, architecture, and intermolecular interactions of asphaltene molecules on properties (self-association and surface activity). *Heliyon* **2022**, *8*, No. e12170.
(2) Sjöblom, J.; Simon, S.; Xu, Z. Model molecules mimicking asphaltenes. *Advances in colloid and interface science* **2015**, *218*, 1−16.
(3) Mullins, O. C.; Sabbah, H.; Eyssautier, J.; Pomerantz, A. E.; Barré, L.; Andrews, A. B.; Zare, R. N. Advances in asphaltene science and the Yen−Mullins model. *Energy Fuels* **2012**, *26* (7), 3986−4003.
(4) Groenzin, H.; Mullins, O. C. Molecular size and structure of asphaltenes from various sources. *Energy Fuels* **2000**, *14* (3), 677−684.
(5) Alimohammadi, S.; Zendehboudi, S.; James, L. A comprehensive review of asphaltene deposition in petroleum reservoirs: Theory, challenges, and tips. *Fuel* **2019**, *252*, 753−791.
(6) Adams, J. J. Asphaltene adsorption, a literature review. *Energy Fuels* **2014**, *28* (5), 2831−2856.
(7) Dudasov, D.; Simon, S. B.; Hemmingsen, P. L. V.; Sjöblom, J. Study of asphaltenes adsorption onto different minerals and clays. *Colloids Surf., A* **2008**, *317* (1−3), 1−9.
(8) Leon, O.; Rogel, E.; Espidel, J.; Torres, G. Asphaltenes: structural characterization, self-association, and stability behavior. *Energy Fuels* **2000**, *14* (1), 6−10.
(9) Kim, S. T., Boudh-Hir, M. E., Mansoori, G. A. (1990). *The Role of Asphaltene in Wettability Reversal*. In SPE Annual Technical Conference and Exhibition. OnePetro.
(10) Anderson, W. G. Wettability literature survey-part 1: rock/oil/brine interactions and the effects of core handling on wettability. *Journal of petroleum technology* **1986**, *38* (10), 1125−1144.
(11) Buckley, J. S.; Liu, Y.; Monsterleet, S. Mechanisms of wetting alteration by crude oils. *SPE journal* **1998**, *3* (01), 54−61.
(12) Amin, J. S.; Nikooee, E.; Ghatee, M. H.; Ayatollahi, S.; Alamdari, A.; Sedghamiz, T. Investigating the effect of different asphaltene structures on surface topography and wettability alteration. *Appl. Surf. Sci.* **2011**, *257* (20), 8341−8349.
(13) Crocker, M. E.; Marchin, L. M. Wettability and adsorption characteristics of crude-oil asphaltene and polar fractions. *Journal of petroleum technology* **1988**, *40* (04), 470−474.
(14) Kaminsky, R., Radke, C. J. *Water Films, Asphaltenes, and Wettability Alteration (No. DOE/FEW-4680)*. Lawrence Berkeley National Lab (LBNL): Berkeley, CA, 1998.
(15) Mullins, O. C. The modified Yen model. *Energy Fuels* **2010**, *24* (4), 2179−2207.
(16) Acevedo, S.; Castillo, J.; Fernández, A.; Goncalves, S.; Ranaudo, M. A. A study of multilayer adsorption of asphaltenes on glass surfaces by photothermal surface deformation. Relation of this adsorption to aggregate formation in solution. *Energy Fuels* **1998**, *12* (2), 386−390.
(17) Marczewski, A. W.; Szymula, M. Adsorption of asphaltenes from toluene on mineral surface. *Colloids Surf., A* **2002**, *208* (1−3), 259−266.
(18) Acevedo, S.; Ranaudo, M. A.; Escobar, G.; Gutiérrez, L.; Ortega, P. Adsorption of asphaltenes and resins on organic and inorganic substrates and their correlation with precipitation problems in production well tubing. *Fuel* **1995**, *74* (4), 595−598.
(19) Acevedo, S.; Ranaudo, M. A.; García, C.; Castillo, J.; Fernández, A. *Energy Fuels* **2003**, *17* (2), 257−261.
(20) Alboudwarej, H.; Pole, D.; Svrcek, W. Y.; Yarranton, H. W. Adsorption of asphaltenes on metals. *Industrial & engineering chemistry research* **2005**, *44* (15), 5585−5592.
(21) Ekholm, P.; Blomberg, E.; Claesson, P.; Auflem, I. H.; Sjöblom, J.; Kornfeldt, A. A quartz crystal microbalance study of the adsorption of asphaltenes and resins onto a hydrophilic surface. *J. Colloid Interface Sci.* **2002**, *247* (2), 342−350.
(22) Dudášová, D.; Silset, A.; Sjöblom, J. Quartz crystal microbalance monitoring of asphaltene adsorption/deposition. *J. Dispersion Sci. Technol.* **2008**, *29* (1), 139−146.
(23) Xie, K.; Karan, K. Kinetics and thermodynamics of asphaltene adsorption on metal surfaces: A preliminary study. *Energy Fuels* **2005**, *19* (4), 1252−1260.
(24) Liu, F.; Hickman, S.; Maqbool, T.; Pauchard, V.; Banerjee, S. Study of Asphaltene Deposition onto Stainless-Steel Surfaces Using Quartz Crystal Microbalance with Dissipation. *Energy Fuels* **2020**, *34* (8), 9283−9295.
(25) Subramanian, S.; Simon, S.; Gao, B.; Sjöblom, J. Asphaltene fractionation based on adsorption onto calcium carbonate: Part 1. Characterization of sub-fractions and QCM-D measurements. *Colloids Surf., A* **2016**, *495*, 136−148.
(26) Tavakkoli, M.; Panuganti, S. R.; Vargas, F. M.; Taghikhani, V.; Pishvaie, M. R.; Chapman, W. G. Asphaltene deposition in different depositing environments: Part 1. *Model oil. Energy & fuels* **2014**, *28* (3), 1617−1628.
(27) Girard, H. L.; Bourrianne, P.; Chen, D.; Jaishankar, A.; Vreeland, J. L.; Cohen, R. E.; McKinley, G. H. Asphaltene adsorption on functionalized solids. *Langmuir* **2020**, *36* (14), 3894−3902.
(28) Salehzadeh, M.; Husein, M. M.; Ghotbi, C.; Taghikhani, V.; Dabir, B. Investigating the role of asphaltenes structure on their aggregation and adsorption/deposition behavior. *Geoenergy Science and Engineering* **2023**, *230*, No. 212204.
(29) Abudu, A.; Goual, L. Adsorption of crude oil on surfaces using quartz crystal microbalance with dissipation (QCM-D) under flow conditions. *Energy Fuels* **2009**, *23* (3), 1237−1248.
(30) Hannisdal, A.; Ese, M. H.; Hemmingsen, P. V.; Sjöblom, J. Particle-stabilized emulsions: Effect of heavy crude oil components pre-adsorbed onto stabilizing solids. *Colloids Surf., A* **2006**, *276* (1−3), 45−58.
(31) Zahabi, A.; Gray, M. R.; Dabros, T. Kinetics and properties of asphaltene adsorption on surfaces. *Energy Fuels* **2012**, *26* (2), 1009−1018.
(32) Dubey, S. T.; Waxman, M. L. Asphaltene adsorption and desorption from mineral surfaces. *SPE Reservoir Engineering* **1991**, *6* (03), 389−395.
(33) Haji-Savameri, M.; Norouzi-Apourvari, S.; Irannejad, A.; Hemmati-Sarapardeh, A.; Schaffie, M.; Mosavi, A. Experimental study and modelling of asphaltene deposition on metal surfaces with superhydrophobic and low sliding angle inner coatings. *Sci. Rep.* **2021**, *11* (1), No. 16812.
(34) Castillo, J.; Goncalves, S.; Fernández, A.; Mujica, V. Applications of photothermal displacement spectroscopy to the study of asphaltenes adsorption. *Optics communications* **1998**, *145* (1−6), 69−75.
(35) Labrador, H.; Fernández, Y.; Tovar, J.; Munoz, R.; Pereira, J. C. Ellipsometry study of the adsorption of asphaltene films on a glass surface. *Energy Fuels* **2007**, *21* (3), 1226−1230.
(36) Hu, X.; Yutkin, M. P.; Hassan, S.; Wu, J.; Prausnitz, J. M.; Radke, C. J. Asphaltene adsorption from toluene onto silica through thin water layers. *Langmuir* **2019**, *35* (2), 428−434.
(37) Willhite, G. P. *Waterflooding*. Society of Petroleum Engineers: Richardson, TX, 1986.
(38) Anderson, W. Wettability literature survey-part 2: Wettability measurement. *Journal of petroleum technology* **1986**, *38* (11), 1246−1262.
(39) Ding, H.; Rahman, S. Experimental and theoretical study of wettability alteration during low salinity water flooding-an state of the art review. *Colloids Surf., A* **2017**, *520*, 622−639.
(40) Vledder, P., Fonseca, J. C., Wells, T., Gonzalez, I., Ligthelm, D. (2010). *Low Salinity Water Flooding: Proof of Wettability Alteration on a Field Wide Scale*. In SPE Improved Oil Recovery Symposium. OnePetro.
(41) Al-Bayati, A.; Karunarathne, C. I.; Al Jehani, A. S.; Al-Yaseri, A. Z.; Keshavarz, A.; Iglauer, S. Wettability alteration during low-salinity water flooding. *Energy Fuels* **2022**, *36* (2), 871−879.

https://doi.org/10.1021/acsomega.3c09294
ACS Omega 2024, 9, 15982−15995

(42) Leach, R. O.; Wagner, O. R.; Wood, H. W.; Harpke, C. F. A laboratory and field study of wettability adjustment in water flooding. *Journal of Petroleum Technology* **1962**, *14* (02), 206−212.
(43) Iglauer, S.; Wu, Y.; Shuler, P.; Tang, Y.; Goddard, W. A., III New surfactant classes for enhanced oil recovery and their tertiary oil recovery potential. *J. Pet. Sci. Eng.* **2010**, *71* (1−2), 23−29.
(44) Iglauer, S.; Paluszny, A.; Rahman, T.; Zhang, Y.; Wülling, W.; Lebedev, M. Residual trapping of CO2 in an oil-filled, oil-wet sandstone core: Results of three-phase pore-scale imaging. *Geophys. Res. Lett.* **2019**, *46* (20), 11146−11154.
(45) Powers, D. P.; Sadeghi, H.; Yarranton, H. W.; Van Den Berg, F. G. A. Regular solution based approach to modeling asphaltene precipitation from native and reacted oils: Part 1, molecular weight, density, and solubility parameter distributions of asphaltenes. *Fuel* **2016**, *178*, 218−233.
(46) Alboudwarej, H.; Beck, J.; Svrcek, W. Y.; Yarranton, H. W.; Akbarzadeh, K. Sensitivity of asphaltene properties to separation techniques. *Energy Fuels* **2002**, *16* (2), 462−469.
(47) Rane, J. P.; Harbottle, D.; Pauchard, V.; Couzis, A.; Banerjee, S. Adsorption kinetics of asphaltenes at the oil−water interface and nanoaggregation in the bulk. *Langmuir* **2012**, *28* (26), 9986−9995.
(48) Sauerbrey, G. J. Z. P. The use of quarts oscillators for weighing thin layers and for microweighing. *Z. Phys.* **1959**, *155*, 206−222.
(49) Kanazawa, K. K.; Gordon, J. G. Frequency of a quartz microbalance in contact with liquid. *Anal. Chem.* **1985**, *57* (8), 1770−1771.
(50) Rodahl, M.; Kasemo, B. On the measurement of thin liquid overlayers with the quartz-crystal microbalance. *Sensors and Actuators A: Physical* **1996**, *54* (1−3), 448−456.
(51) Gonzalez, V.; Taylor, S. E. Asphaltene adsorption on quartz sand in the presence of pre-adsorbed water. *J. Colloid Interface Sci.* **2016**, *480*, 137−145.
(52) Reviakine, I.; Johannsmann, D.; Richter, R. P. Hearing What You Cannot See and Visualizing What You Hear: Interpreting Quartz Crystal Microbalance Data from Solvated Interfaces. *Anal. Chem.* **2011**, *83* (23), 8838−8848.
(53) Andersson, M.; Andersson, J.; Sellborn, A.; Berglin, M.; Nilsson, B.; Elwing, H. Quartz crystal microbalance-with dissipation monitoring (QCM-D) for real-time measurements of blood coagulation density and immune complement activation on artificial surfaces. *Biosens. Bioelectron.* **2005**, *21* (1), 79−86.
(54) Voinova, M. V.; Rodahl, M.; Jonson, M.; Kasemo, B. Viscoelastic acoustic response of layered polymer films at fluid-solid interfaces: continuum mechanics approach. *Physica Scripta* **1999**, *59* (5), 391.
(55) Liu, F.; Darjani, S.; Akhmetkhanova, N.; Maldarelli, C.; Banerjee, S.; Pauchard, V. Mixture effect on the dilatation rheology of asphaltenes-laden interfaces. *Langmuir* **2017**, *33* (8), 1927−1942.
(56) Sztukowski, D. M.; Jafari, M.; Alboudwarej, H.; Yarranton, H. W. Asphaltene self-association and water-in-hydrocarbon emulsions. *J. Colloid Interface Sci.* **2003**, *265* (1), 179−186.
(57) Rudrake, A.; Karan, K.; Horton, J. H. A combined QCM and XPS investigation of asphaltene adsorption on metal surfaces. *J. Colloid Interface Sci.* **2009**, *332* (1), 22−31.
(58) Zhu, B. Y.; Gu, T. Reverse hemimicelle formation of 1-decanol from heptane at the solution/graphite interface. *Colloids Surf.* **1990**, *46* (2), 339−345.
(59) Rane, J. P.; Pauchard, V.; Couzis, A.; Banerjee, S. Interfacial rheology of asphaltenes at oil−water interfaces and interpretation of the equation of state. *Langmuir* **2013**, *29* (15), 4750−4759.
(60) Rane, J. P.; Zarkar, S.; Pauchard, V.; Mullins, O. C.; Christie, D.; Andrews, A. B.; Banerjee, S. Applicability of the Langmuir equation of state for asphaltene adsorption at the oil−water interface: Coal-derived, petroleum, and synthetic asphaltenes. *Energy Fuels* **2015**, *29* (6), 3584−3590.
(61) Zarkar, S.; Pauchard, V.; Farooq, U.; Couzis, A.; Banerjee, S. Interfacial Properties of Asphaltenes at Toluene - Water Interfaces. *Langmuir.* **2015**, *31*, 4878−4886.
(62) Pauchard, V.; Rane, J. P.; Banerjee, S. Asphaltene-laden interfaces form soft glassy layers in contraction experiments: A mechanism for coalescence blocking. *Langmuir* **2014**, *30* (43), 12795−12803.
(63) de la Cruz, J. L. M.; Castellanos-Ramírez, I. V.; Ortiz-Tapia, A.; Buenrostro-González, E.; Durán-Valencia, C. D. L. A.; López-Ramírez, S. Study of monolayer to multilayer adsorption of asphaltenes on reservoir rock minerals. *Colloids Surf., A* **2009**, *340* (1−3), 149−154.
(64) Filippov, L. K. Dynamic surface tension of aqueous surfactant solutions: 2. Diffusion-kinetic-convective controlled adsorption. *J. Colloid Interface Sci.* **1994**, *164* (2), 471−482.
(65) Johnson, P. R.; Elimelech, M. Dynamics of colloid deposition in porous media: Blocking based on random sequential adsorption. *langmuir* **1995**, *11* (3), 801−812.
(66) Wang, J. S.; Nielaba, P.; Privman, V. Collective effects in random sequential adsorption of diffusing hard squares. *Mod. Phys. Lett. B* **1993**, *7* (3), 189−196.
(67) Swendsen, R. H. Dynamics of random sequential adsorption. *Phys. Rev. A* **1981**, *24* (1), 504.
(68) Lee, J. W.; Hong, B. H. Irreversible sequential adsorption of k-mers with diffusional relaxation on a one-dimensional lattice. *J. Chem. Phys.* **2003**, *119* (1), 533−537.
(69) Rostami, P.; Mehraban, M. F.; Sharifi, M.; Dejam, M.; Ayatollahi, S. Effect of water salinity on oil/brine interfacial behaviour during low salinity waterflooding: A mechanistic study. *Petroleum* **2019**, *5* (4), 367−374.
(70) Vijapurapu, C. S.; Rao, D. N. Compositional effects of fluids on spreading, adhesion and wettability in porous media. *Colloids Surf., A* **2004**, *241* (1−3), 335−342.

https://doi.org/10.1021/acsomega.3c09294
ACS Omega 2024, 9, 15982−15995